Energy & Environmental Science

ROYAL SOCIETY OF CHEMISTRY

COMMUNICATION

View Article Online
View Journal | View Issue

Check for updates

Cite this: *Energy Environ. Sci.*, 2021, **14**, 900

Received 25th August 2020,
Accepted 14th January 2021

DOI: 10.1039/d0ee02730h

rsc.li/ees

Solar-driven ionic power generation *via* a film of nanocellulose @ conductive metal–organic framework†

Shengyang Zhou, [a] Zhen Qiu, [b] Maria Strømme *[a] and Chao Xu *[a]

Solar energy fits well with the increasing demand for clean sustainable energy. This paper describes a freestanding hybrid film composed of a conductive metal–organic framework layered on cellulose nanofibres which enables efficient solar power generation. The working principle, which is different from the mechanisms of traditional photovoltaic or solid-state thermoelectric generation systems, is based on ionic thermophoresis and electrokinetic effects. Given the strong light absorption and low thermal conductivity of the film, a large thermal gradient can be produced on the surface under light illumination to induce fast water evaporation in an aqueous electrolyte. The thermal gradient and the water evaporation drive selective ion transport through the charged nanochannels, which generates ionic thermoelectric and streaming potentials, respectively. The assembled device can produce a sustained voltage output of ~1.1 V, with a high power density of up to 15 W m^{-2} under one sun illumination. This study provides a new route for solar power generation.

Broader context

Solar energy and water are the most abundant resources in nature. Most of the solar energy absorbed by the Earth's surface converts into heat, and about half of this thermal energy drives natural water evaporation. Therefore, it is highly desirable to develop novel technologies and materials to take advantages of the abundant solar thermal resource and the induced water evaporation in nature for power generation. We herein report a new technology of "solar-driven ionic power generation" based on ionic thermophoresis and electrokinetic effects that could convert solar energy into electricity by using a film of nanocellulose @ conductive metal–organic framework. The hybrid film enables the formation of a large thermal gradient on the surface of the film under light illumination. This gradient further induces fast water evaporation in a NaCl aqueous electrolyte. The thermal gradient and the water evaporation could drive selective ion transport through the charged nanochannels, which generates a high ionic voltage up to 1.1 V. This technology not only provides a new approach for solar power generation, but also may find applications in solar steam generation, seawater desalination, and self-powered wearable electronics.

Introduction

Current technology for converting solar energy into electricity is mostly based on the photovoltaic effect associated with the generation of electrons and holes in solid semiconductors.[1] In fact, most of the solar energy absorbed by the Earth's surface converts into heat, and about half of this thermal energy drives natural water evaporation.[2,3] As we know, applying a thermal gradient across an electrolyte can result in a thermophoretic mobility difference between the cations and anions as a result of the Soret effect.[4,5] As well, the flow of electrolyte on a charged solid surface driven by an external stimulus (*e.g.*, a pressure gradient, evaporation, transpiration) can cause accumulation of counter-ions along the direction of the flow, which is usually understood as an electrokinetic effect.[6–8] Thus, the Soret and electrokinetic effects both induce asymmetrical distribution of the ions in the electrolyte, which gives rise to the formation of a potential gradient.[9] In this context, the development of an integrated system that enables solar heat harvest and ion transport regulation could take advantage of both the abundant solar thermal resource and the induced water evaporation in nature to generate electricity, which would provide an alternative technological method for solar power generation.

In general, solar thermal evaporation can be realized by the use of photothermal conversion materials,[10] which usually require interconnected channels or porous structures to facilitate water transport and continuous vapour generation. These channels can then be used to transport electrolytes. In particular, by tuning the dimensions of the channels close to the Debye length and introducing surface charges onto the channel walls, enhanced selective diffusion and accelerated transport of electrolyte ions can be achieved in the confined nanochannels.[11,12] This so-called

[a] *Nanotechnology and Functional Materials, Department of Materials Sciences and Engineering, The Ångström Laboratory, Uppsala University, Uppsala 751 03, Sweden. E-mail: maria.stromme@angstrom.uu.se, chao.xu@angstrom.uu.se*
[b] *Solid State Physics, Department of Materials Sciences and Engineering, The Ångström Laboratory, Uppsala University, Uppsala 751 03, Sweden*

† Electronic supplementary information (ESI) available. See DOI: 10.1039/d0ee02730h

nanofluidic effect can produce a significantly greater electrical output than that derived from the bulk counterparts, based on classical Soret and electrokinetic effects.[13–17] Therefore, the design of charged nanochannels with tailored dimensions in photothermal conversion materials plays a key role in realizing the solar-driven ionic power generation (IPG) process.

Here, we present a hierarchical porous hybrid film composed of nanofibres of cellulose on which conductive metal–organic frameworks have been layered to enable photothermal conversion and regulation of ion transport that can harvest solar energy for generation of electricity. The cellulose nanofibre @ conductive metal–organic framework (CCM) film has a charged nanoporous structure, high electrical conductivity and low thermal conductivity. Light absorption by the film after infiltration with aqueous electrolytes produces heat and drives fast water evaporation, which simultaneously induce ionic thermoelectric and streaming potentials. This synergistic effect gives rise to a sustained ionic voltage of ~1.1 V with a power density of up to 15 W m^{-2}.

Preparation and characterization of the CCM film

The hybrid nanofibres are prepared by interfacial synthesis of a conductive metal–organic framework Ni_3(2,3,6,7,10,11-hexaiminotriphenylene)$_2$ (Ni-HITP) onto cellulose nanofibres extracted from *Cladophora* algae.[18,19] After introducing carboxyls onto the surface of the cellulose by TEMPO (2,2,6,6-tetramethylpiperidin-1-yloxyl) oxidation, the nanofibres can induce continuous growth of Ni-HITP nanolayers by complexing of $NiCl_2$ with the HITP linker (Shanghai Tensus Bio-Tech) in an aqueous ammonium solution with an air flow (Fig. 1a and Fig. S1, ESI†). The composition of the obtained CCM nanocomposite was determined by powder X-ray diffraction, thermogravimetric and X-ray photoelectron spectroscopy analyses (Fig. S2a–c, ESI†). The transmission electron microscopy (TEM) image shown in Fig. 1b illustrates a typical core–shell structure, where the Ni-HITP nanolayer, with a thickness of ~18 nm, wraps around the *Cladophora* nanofibre. The high-resolution TEM image of the Ni-HITP nanolayer shows ordered nanopores with a diameter of ~2 nm in a hexagonal arrangement. These nanofibrous structures allow the nanocomposites to be easily processed. Dispersion of the CCM nanofibres in water results in a homogeneous suspension that can be easily fabricated into a flexible, freestanding film by vacuum filtration (Fig. 1c and Fig. S1, ESI†). As shown in the scanning electron microscopy (SEM) image in Fig. 1d, stacking and interweaving of the nanofibres form a uniform CCM film with a thickness of ~5 μm. Nitrogen sorption measurement has revealed the hierarchical porous structure of the film; the micropores (~2 nm) and mesopores (5–60 nm) are derived from the microporous framework of Ni-HITP and the inter-fibre structures, respectively (Fig. S2d and S3, ESI†). The water contact angle of the film (~9.7°), the result of the presence of cellulose, indicates its hydrophilic nature (Fig. 1c). The electrical conductivity of the film was measured to be 97.5 S cm^{-1} (Fig. S2e, ESI†). In addition, the film is highly physically stable in the electrolyte; no deformation or breakages were observed after immersing a piece of the film into 1 M NaCl aqueous solution with stirring for one week (Fig. S2f, ESI†).

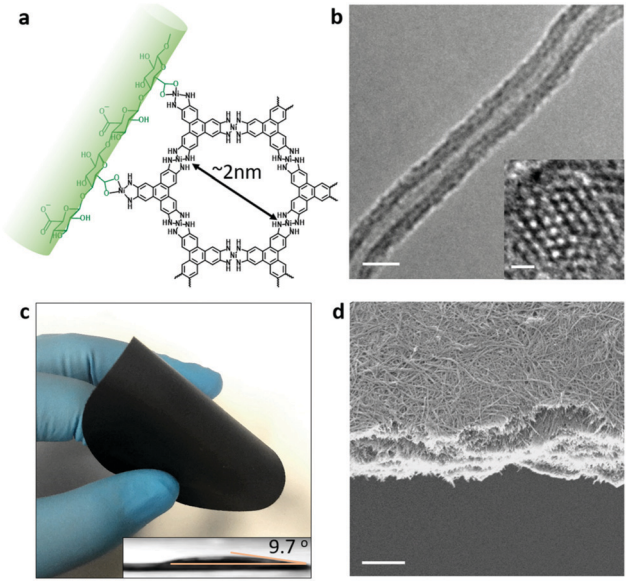

Fig. 1 Structure of the conductive metal–organic framework layered on cellulose nanofibre and the assembled film. (a) Molecular structure and (b) transmission electron microscopy (TEM) image of a CCM hybrid nanofibre (scale bar: 50 nm); the inset shows a high resolution TEM image of the conductive metal–organic framework Ni_3(2,3,6,7,10,11-hexaiminotriphenylene)$_2$ (Ni-HITP) nanolayer (scale bar: 5 nm). (c) Demonstration of the flexibility of the film; the inset shows the water contact angle. (d) Cross-sectional scanning electron microscopy image of the film (scale bar: 5 μm).

Solar thermal conversion in and water evaporation from the CCM film

Ultraviolet-visible-near infrared absorption spectra have shown that the CCM film strongly absorbs light (>90%) throughout the solar spectrum range (Fig. 2a) as a result of the highly conjugated molecular structure of Ni-HITP.[20] Because of its efficient solar absorption and the photothermal activity of the metal–organic framework, we expected that the CCM film would serve as a good solar absorber for photothermal conversion. When the film was floated on water ($T \approx 17$ °C) and illuminated under one sun (1 kW m^{-2}), the surface temperature of the film reached ~51 °C in 10 min (Fig. 2b). The infrared

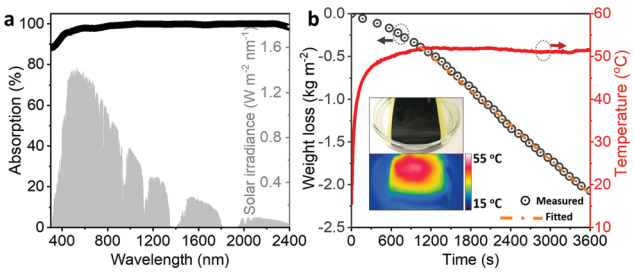

Fig. 2 Light absorption by and solar thermal evaporation from the hybrid cellulose nanofibre @ conductive metal–organic framework (CCM) film. (a) Ultraviolet-visible-near infrared absorption spectra for the CCM film and the solar spectrum (AM 1.5G). (b) Time-dependent surface temperature of the CCM film and the loss of water from the CCM film under one sun illumination. The infrared image shows the temperature distribution on the film surface after illumination for 20 min.

image shows that the local temperature of the film was significantly higher than that of the surroundings, with a thermal gradient of ~35 °C at the interface between the film and the water. This high thermal gradient can be attributed to the low thermal conductivity of the film (0.045 W m^{-1} K^{-1}; Fig. S4, ESI†). This value is far below those for other materials used for solar photothermal conversion such as carbons, metal nanoparticles, and organic polymers (0.4–100 W m^{-1} K^{-1}).[3,21,22] The low thermal conductivity prevents heat conduction, resulting in efficient heat localization. In combination with its hydrophilicity and hierarchical porous structure, the film exhibits highly efficient solar thermal steam generation at a rate of 2.42 kg m^{-2} h^{-1} under one sun illumination, which is much higher than the evaporation rate of bulk water under the same conditions (~0.5 kg m^{-2} h^{-1}).[10,21] The solar thermal evaporation rate is also higher than the reported values for traditional photothermal conversion materials such as carbon, semiconductor, and metal nanoparticle, and is comparable to those for state-of-the-art nanoporous systems (Table S1, ESI†). The vaporization enthalpy of the water in the CCM film was consistently lower than that of a pure cellulose film and bulk water, as indicated by differential scanning calorimetry measurements (Fig. S5a and b, ESI†).[23,24] The reduction of vaporization enthalpy of water in confined systems is also observed in previous studies.[24–26] In addition, studies using infrared spectroscopy have suggested the formation of water clusters in the CCM film as a result of the confinement of water in the microporous Ni-HITP framework (Fig. S5c, ESI†).[27] Previous studies by simulation[27] and crystallography[28] methods have also revealed the water cluster confinement in the porous channels of related MOF structures. Therefore, we speculate that the water molecules evaporate from the CCM film in the form of water clusters rather than as individual molecules as would be the case for bulk water and a mesoporous cellulose film without, or with less, nano-confinement.[29] Furthermore, a COMSOL simulation study has indicated that the nanoporous structures in the film greatly facilitate water transport during the solar-thermal evaporation process (Fig. S6, ESI†). Collectively, the ability of the CCM film to efficiently generate steam using solar thermal energy can be explained by the synergistic activity of photothermal conversion, hydrophilicity, hierarchical porosity, and the nano-confinement effect.

Charged nanochannels in the CCM film

The ionic conduction behaviour of the CCM film along the in-plane direction was investigated using a home-made apparatus (Fig. S7a and b, ESI†). The plots of the ionic conductivity of the film *versus* the NaCl concentration in the electrolyte at different pH values are shown in Fig. 3a. For comparison, the conductivity of bulk NaCl solution (pH = 7) at different concentrations was also measured. As expected, the conductivity of the bulk NaCl solution was proportional to the NaCl concentration (Fig. S7c, ESI†). In comparison, the conductivity of the film in the electrolyte (pH = 7) with high NaCl concentrations ($>10^{-3}$ M) was similar to that of the bulk NaCl solution at high concentrations. However, it slightly deviated from the conductivity of the bulk NaCl solution at low concentrations ($<10^{-3}$ M). In addition, the deviation became more significant with increasing acidity or basicity of the electrolyte, and the plots

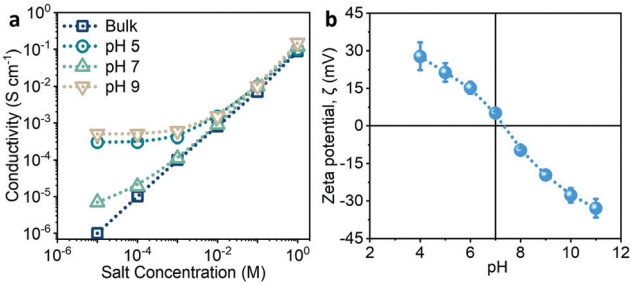

Fig. 3 Ionic conduction and charged nanostructure in the hybrid cellulose nanofibre @ conductive metal–organic framework (CCM) film. (a) The ionic conductivity of the CCM film as a function of the salt concentration measured at different pH values (aqueous NaCl electrolyte). (b) Measured zeta potentials of the CCM nanofibres (0.01 M NaCl) at different pH values.

gradually approached plateaus at low NaCl concentrations. These results suggest that the ion transport was governed by the surface-charged nanochannels in the CCM film under acidic or basic conditions.[30,31] The formation of surface charges was confirmed by measuring the zeta potential of the CCM nanofibres as H^+ or OH^- could be doped to the Ni-HITP framework (Fig. 3b). The charged surface subsequently attracts electrolyte ions with the opposite charge (counter-ions) to form electrical double layers (EDLs), while repelling ions with the same charge (co-ions). Since the mesopore size of the CCM film is comparable with the Debye length of the electrolyte ions at low NaCl concentrations (Fig. S7d, ESI†), the EDLs on the walls overlap and the mesopores are mainly filled with counter-ions.[15] The selective transport of electrolyte ions in the charged nanochannels follows typical nanofluidic behaviour.[11,32]

Solar-driven ionic power generation

Because of the formation of a charged surface on the nanoporous CCM film when it is infiltrated by a non-neutral electrolyte, the streaming potential can theoretically be generated during the evaporation of water from the electrolyte.[33] In order to realize the generation of streaming potential, we dropped the electrolyte onto one side of the film (Fig. 4a and Video S1, ESI†). The resulting wet–dry interface generated an electrical potential difference by causing the asymmetrical distribution of cations and anions, driven by the selective transport of ions in the charged nanochannels of the CCM film during water evaporation. The voltage between the wet and dry sides was measured using a source meter. The *x*-intercept of the recorded current–voltage (*I*–*V*) curve gives the value of the open-circuit voltage. Firstly, the pH value of the electrolyte (the NaCl concentration was fixed at 0.01 M) had a significant influence on the value and direction of the voltage (Fig. 4a and Fig. S8, ESI†). The absolute value of the voltage increased with increasing acidity or basicity. On the other hand, the voltage was oppositely directed in acidic and basic electrolytes. This can be explained by the fact that the pH value affects the density and sign of the surface charges on the CCM film, as revealed by the zeta potential studies, which further determines the absolute value and sign of the generated voltage. As expected, dropping pure

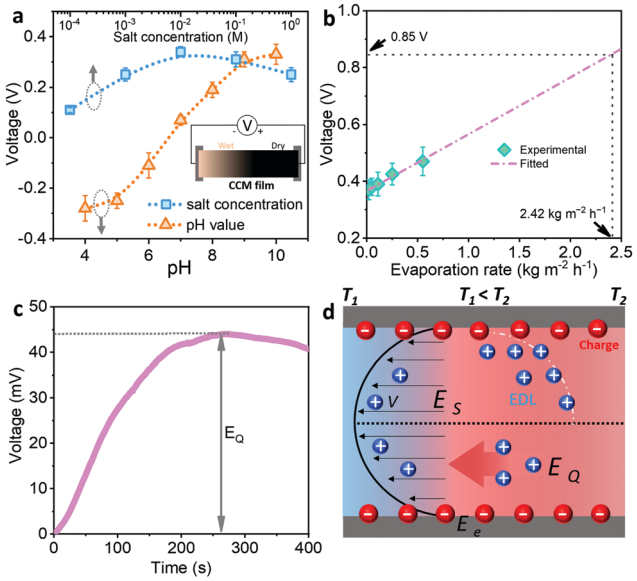

Fig. 4 Investigation of the contributions of ionic voltage. (a) The streaming potential generated in the hybrid cellulose nanofibre @ conductive metal–organic framework (CCM) film at different pH values (where the NaCl concentration in the aqueous electrolyte was fixed at 0.01 M) and different salt concentrations (where the pH value of the electrolyte was fixed at 10). (b) The dependence of the streaming potential on the water evaporation rate. The electrolyte NaCl concentration and pH value were fixed at 0.01 M and 10, respectively. (c) The measured ionic thermoelectric voltage in the CCM film, at a thermal gradient of 5 °C. (d) A schematic of ion distribution and transport in the charged nanochannels of the CCM film and the proposed mechanisms for voltage generation.

water onto the film resulted in a relatively low voltage (~0.05 V) because no charge was formed on the surface of the film in a neutral electrolyte. In addition, the salt concentration of the electrolyte had only minor influence on the voltage (blue dots in Fig. 4a). Since the salt concentration mainly affects the permittivity of the electrolyte and the Debye diameter of ions, and the two factors have an opposite effect on the streaming potential.[6] The plotted curve of voltage *versus* salt concentration is parabolic (the pH value was fixed at 10). On this basis, a maximum voltage of 0.35 V was achieved under ambient conditions by adjusting the pH value (10) and NaCl concentration (0.01 M) of the electrolyte. Furthermore, the fast evaporation rate promoted the movement and accumulation of counter-ions on the charged surface. As a result, the voltage was linearly proportional to the water evaporation rate (Fig. 4b), which is consistent with theoretical predictions and reported experimental results.[6,7]

When exposing the wet side of the CCM film to one sun illumination, the open-circuit voltage significantly increased to ~1.1 V in 10 min (Fig. S9 and Video S2, ESI†). Since the water evaporation rate in the CCM film under sun illumination was 2.42 kg m^{-2} h^{-1}, the contribution of streaming potential was predicted to be 0.85 V by extrapolating the linear curve in Fig. 4b. The difference between the overall voltage (1.1 V) and the estimated streaming potential (0.85 V) can probably be attributed to the contribution of ionic thermoelectric voltage. As mentioned above, the charged nanochannels in the CCM film are able to selectively transport electrolyte ions, and the difference in mobility between the anions and cations can be amplified by applying a thermal gradient across the film. The good photothermal conversion ability allowed a large thermal gradient (~35 °C) to be generated between the wet and dry sides under one illumination, which could potentially generate the ionic thermoelectric response. In order to test this speculation, we designed an apparatus to apply a temperature difference of 5 °C between the two sides of the CCM film (17 *vs.* 22 °C) infiltrated with electrolyte (0.01 M NaCl, pH = 10); the film was sealed in a coffee-bag arrangement to avoid water evaporation. The potential difference between the warm and cold sides was monitored by an electrochemical instrument (Fig. S10, ESI†). The voltage gradually increased with time and reached a peak of 43 mV at 250 s (Fig. 4c). The thermal gradient-induced voltage can be explained by an ionic Seebeck effect (analogous to the classical Seebeck effect of thermoelectric materials). The ionic Seebeck coefficient of the film was calculated to be 8.5 mV K^{-1} according to the equation $S = \Delta V/\Delta T$, where S is ionic Seebeck coefficient, ΔV is the open-circuit voltage, and ΔT is the temperature difference.[34] Therefore, the ionic thermoelectric voltage generated in the CCM film under one sun illumination was calculated to be ~0.3 V, close to the differential value (0.25 V) between the overall voltage and the estimated streaming potential. In contrast, the electronic Seebeck coefficient of CCM films was measured to be −11.5 μV K^{-1} (Fig. S11, ESI†),[35] which is three orders of magnitude lower than the ionic Seebeck coefficient, indicating that the electronic Seebeck effect on the overall voltage was negligible. Therefore, the CCM film enables the generation of both streaming potential and ionic thermoelectric voltage driven by solar thermal water evaporation, resulting in the high overall voltage output of ~1.1 V.

In order to demonstrate the structural advantages of the CCM film for solar-driven IPG, we compared these results to those from other materials used for power generation under the same conditions. The film prepared by blending Ni-HITP particles with nanocellulose (Fig. S12, ESI†) gave no significant response (voltage < 0.02 V) because of the associated high electrical resistance and the discontinuous charged surfaces. Although the film prepared by mixing multi-walled carbon nanotubes (MWCNTs) with nanocellulose resulted in relatively high electrical conductivity, the voltage output was very low (<0.03 V) because of the neutral charged surface of MWCNTs (Fig. S13, ESI†). Interestingly, replacing the MWCNT with carboxylated MWCNTs in the film resulted in a voltage output of ~0.3 V under ambient conditions because the water evaporation on the charged CNT surface induced the streaming potential. However, no significant increase in voltage was observed when the film was exposed to one sun illumination, indicating that there was no ionic thermoelectric output because of the high thermal conductivity of CNTs. We also prepared a film by growing poly(3,4-ethylenedioxythiophene):poly (4-styrenesulfonate) (PEDOT:PSS), with both high electronic and high ionic conductivity, on nanocellulose (Fig. S14, ESI†). The morphology and mesoporous structure of this film were similar to those of the CCM film. However, there was no

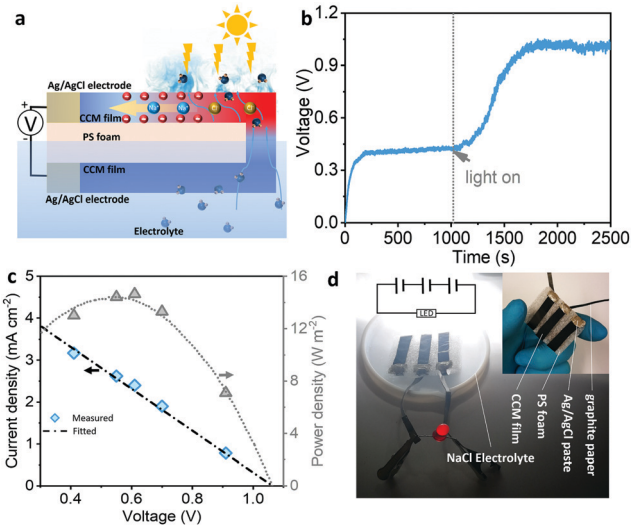

Fig. 5 Proof-of-concept design for a solar power generation device. (a) Schematic of the device. (b) Measured open-circuit voltage of the device over time with and without light illumination. (c) Current density–voltage curve and calculated power density of the device under one sun illumination. (d) Photo of a red LED powered by a series of devices under one sun illumination. CCM = cellulose nanofibre @ conductive metal–organic framework; PS = polystyrene.

response in terms of streaming potential, probably because the film lacked free charges on the surface. Upon one sun illumination, the PEDOT:PSS/nanocellulose film generated a voltage output of up to ~0.15 V (the temperature gradient was ~30 °C) due to the ionic Soret effect (Fig. S12, ESI†).[34] This value was much lower than that generated in the CCM film (~0.3 V) because the absence of charged nanochannels in the PEDOT:PSS/nanocellulose film impeded the selective transport of electrolyte ions. In addition, we also applied wood nanocellulose (WNC) as the substrate to prepare a CCM film (Fig. S15, ESI†). Interestingly, the WNC-based CCM film enabled the generation of a relatively high streaming potential of ~0.25 V under ambient conditions, which was comparable to the value of ~0.35 V obtained by using the *Cladophora* cellulose-based CCM film. However, the overall voltage output could only reach up to ~0.4 V under one-sun illumination, which most likely can be attributed to the lack of mesopores in the WNC-based CCM film. From these results, we conclude that good photothermal conversion ability, low thermal conductivity, high electrical conductivity, and charged nanochannels in the material are key factors for achieving efficient solar-driven IPG (Fig. 4d).

Proof-of-concept device

We have designed a solar-driven IPG device based on the CCM film (Fig. 5a). A piece of CCM film (1.0 cm × 0.2 cm) was bent to a U-shape and bound onto a piece of polystyrene foam. The two terminals of the film were sealed by an Ag/AgCl gel electrode and then connected with graphite paper as conductive wires. The whole device was floated on an aqueous electrolyte (0.01 M NaCl, pH = 10) and half of the film was soaked in the electrolyte. The open-circuit voltage between the two terminals of the film was recorded during water evaporation. The device generated a voltage output of up to 0.35 V under ambient conditions (Fig. 5b). Significantly, the voltage gradually increased to ~1.1 V in 15 min when the wet side of the device surface was illuminated by a solar simulator (one sun). It seems that neither tuning the thickness of the film nor increasing the MOF content significantly influences the voltage output (Fig. S16, ESI†). Remarkably, there was no significant fluctuation of the output over time and the voltage remained steady at ~1.1 V for 48 h (Fig. S17, ESI†). The high stability can be explained by two factors: (1) the sustained water supply and the fast water evaporation through the film formed a constant wet–dry interface for generating the streaming potential; (2) the low thermal conductivity of the film enabled the formation of a stable thermal gradient across the film for the ionic thermoelectric voltage output. The power density of the device was calculated as ~15 W m^{-2} from the current density–voltage curve (Fig. 5c). This value is significantly larger than that for many other materials used for IPG (Tables S2 and S3, ESI†). In addition, three devices assembled in series (~3 V) were capable of powering a red light-emitting diode under one sun illumination (Fig. 5d).

Conclusions

In summary, we have described a CCM film with the following integrated properties: hierarchical porosity, low thermal conductivity, high electronic conductivity, and efficient photothermal conversion. The pore surface can be doped with an acidic or basic aqueous electrolyte to form charged nanoporous channels. Light illumination of the film generates a thermal gradient and induces water evaporation that drives selective ion transport through the charged nanochannels across the hot–cold and wet–dry interface, respectively. The synergistic effect of this is a high voltage output of ~1.1 V and a high power density of ~15 W m^{-2}. These results demonstrate the great potential of this novel approach to solar-driven IPG by regulating ion transport in charged nanochannels. This study, to the best of our knowledge, is the first example that enables the generation and integration of ionic thermoelectric and streaming potentials in a nanodevice. Further studies will focus on the design of conductive metal–organic frameworks or other porous frameworks with intrinsically charged surfaces that may further enhance the efficiency of power generation. This will also extend the applicability of this technology for use with various electrolytes (*e.g.*, pure water, seawater) for solar-driven IPG. In addition, the technology described in this report could find new applications in solar steam generation, seawater desalination, and self-powered wearable electronics.

Author contributions

S. Z. and C. X. conceived the idea and designed the experiments. S. Z. contributed to material preparation and most characterizations. Z. Q. contributed to the measurements of light

absorption spectrum and zeta potential. S. Z., C. X. and M. S. wrote the manuscript.

Conflicts of interest

The authors declare no competing financial interests.

Acknowledgements

This project was supported by an Åforsk research grant (19-493). Shengyang Zhou acknowledges the China Scholarship Council for financial support. The authors thank Dr Uwe Zimmermann for providing the solar simulator, Dr Zhaohui Wang and Xueying Kong for the kind help with materials synthesis, and Dr Shuangshuang Zeng for the fruitful discussion on COMSOL simulation.

Notes and references

1 N. S. Lewis, *Science*, 2007, **315**, 798–801.
2 A.-H. Cavusoglu, X. Chen, P. Gentine and O. Sahin, *Nat. Commun.*, 2017, **8**, 1–9.
3 H. Ghasemi, G. Ni, A. M. Marconnet, J. Loomis, S. Yerci, N. Miljkovic and G. Chen, *Nat. Commun.*, 2014, **5**, 4449.
4 H. Tyrrell and R. Colledge, *Nature*, 1954, **173**, 264–265.
5 D. Zhao, H. Wang, Z. U. Khan, J. Chen, R. Gabrielsson, M. P. Jonsson, M. Berggren and X. Crispin, *Energy Environ. Sci.*, 2016, **9**, 1450–1457.
6 M. Elimelech, W. H. Chen and J. J. Waypa, *Desalination*, 1994, **95**, 269–286.
7 G. Xue, Y. Xu, T. Ding, J. Li, J. Yin, W. Fei, Y. Cao, J. Yu, L. Yuan, L. Gong, J. Chen, S. Deng, J. Zhou and W. Guo, *Nat. Nanotechnol.*, 2017, **12**, 317–321.
8 J. Yin, X. Li, J. Yu, Z. Zhang, J. Zhou and W. Guo, *Nat. Nanotechnol.*, 2014, **9**, 378–383.
9 K. Xiao, L. Jiang and M. Antonietti, *Joule*, 2019, **3**, 2364–2380.
10 P. Tao, G. Ni, C. Song, W. Shang, J. Wu, J. Zhu, G. Chen and T. Deng, *Nat. Energy*, 2018, **3**, 1031–1041.
11 L. Bocquet and E. Charlaix, *Chem. Soc. Rev.*, 2010, **39**, 1073–1095.
12 A. Siria, M.-L. Bocquet and L. Bocquet, *Nat. Rev. Chem.*, 2017, **1**, 0091.
13 M. Dietzel and S. Hardt, *Phys. Rev. Lett.*, 2016, **116**, 225901.
14 L. Fu, L. Joly and S. Merabia, *Phys. Rev. Lett.*, 2019, **123**, 138001.
15 T. Li, X. Zhang, S. D. Lacey, R. Mi, X. Zhao, F. Jiang, J. Song, Z. Liu, G. Chen, J. Dai, Y. Yao, S. Das, R. Yang, R. M. Briber and L. Hu, *Nat. Mater.*, 2019, **18**, 608–613.
16 F. H. van der Heyden, D. Stein and C. Dekker, *Phys. Rev. Lett.*, 2005, **95**, 116104.
17 A. Siria, P. Poncharal, A.-L. Biance, R. Fulcrand, X. Blase, S. T. Purcell and L. Bocquet, *Nature*, 2013, **494**, 455–458.
18 S. Zhou, L. Nyholm, M. Strømme and Z. Wang, *Acc. Chem. Res.*, 2019, **52**, 2232–2243.
19 S. Zhou, X. Kong, B. Zheng, F. Huo, M. Strømme and C. Xu, *ACS Nano*, 2019, **13**, 9578–9586.
20 D. Sheberla, L. Sun, M. A. Blood-Forsythe, S. L. Er, C. R. Wade, C. K. Brozek, A. N. Aspuru-Guzik and M. Dinca, *J. Am. Chem. Soc.*, 2014, **136**, 8859–8862.
21 C. Chen, Y. Kuang and L. Hu, *Joule*, 2019, **3**, 683–718.
22 O. Bubnova, Z. U. Khan, A. Malti, S. Braun, M. Fahlman, M. Berggren and X. Crispin, *Nat. Mater.*, 2011, **10**, 429–433.
23 X. Zhou, F. Zhao, Y. Guo, B. Rosenberger and G. Yu, *Sci. Adv.*, 2019, **5**, eaaw5484.
24 F. Zhao, X. Zhou, Y. Shi, X. Qian, M. Alexander, X. Zhao, S. Mendez, R. Yang, L. Qu and G. Yu, *Nat. Nanotechnol.*, 2018, **13**, 489–495.
25 Y. Guo, X. Zhao, F. Zhao, Z. Jiao, X. Zhou and G. Yu, *Energy Environ. Sci.*, 2020, **13**, 2087–2095.
26 Q. Lu, W. Shi, H. Yang and X. Wang, *Adv. Mater.*, 2020, **32**, 2001544.
27 N. Nijem, P. Canepa, U. Kaipa, K. Tan, K. Roodenko, S. Tekarli, J. Halbert, I. W. Ostwald, R. K. Arvapally, C. Yang, T. Thonhauser, M. A. Omary and Y. J. Chabal, *J. Am. Chem. Soc.*, 2013, **135**, 12615–12626.
28 X.-Y. Dong, B. Li, B.-B. Ma, S.-J. Li, M.-M. Dong, Y.-Y. Zhu, S.-Q. Zang, Y. Song, H.-W. Hong and T. C. W. Mark, *J. Am. Chem. Soc.*, 2013, **135**, 10214–10217.
29 L. Sun, J. Liu, Y. Zhao, J. Xu and Y. Li, *Carbon*, 2019, **145**, 352–358.
30 K. Raidongia and J. Huang, *J. Am. Chem. Soc.*, 2012, **134**, 16528–16531.
31 S. Qin, D. Liu, G. Wang, D. Portehault, C. J. Garvey, Y. Gogotsi, W. Lei and Y. Chen, *J. Am. Chem. Soc.*, 2017, **139**, 6314–6320.
32 W. Sparreboom, A. van den Berg and J. C. Eijkel, *Nat. Nanotechnol.*, 2009, **4**, 713–720.
33 T. G. Yun, J. Bae, A. Rothschild and I.-D. Kim, *ACS Nano*, 2019, **13**, 12703–12709.
34 H. Wang, U. Ail, R. Gabrielsson, M. Berggren and X. Crispin, *Adv. Energy Mater.*, 2015, **5**, 1500044.
35 L. Sun, B. Liao, D. Sheberla, D. Kraemer, J. Zhou, E. A. Stach, D. Zakharov, V. Stavila, A. A. Talin, Y. Ge, M. D. Allendorf, G. Chen, F. Léonard and M. Dincă, *Joule*, 2017, **1**, 168–177.